Scanning Electrochemical Microscopy #54. Application To The Study Of Heterogeneous Catalytic Reactions—Hydrogen Peroxide Decomposition

José L. Fernández, Cedric Hurth, and Allen J. Bard*

Department of Chemistry and Biochemistry, Center for Nano and Molecular Science and Technology, The University of Texas at Austin, Austin, Texas 78712

Received: January 19, 2005; In Final Form: March 11, 2005

A scanning electrochemical microscopy (SECM) approach for the analysis of heterogeneous catalytic reactions at solid−liquid interfaces is described and applied. In this scheme, reactant, generated at a tip, undergoes a reaction (e.g., disproportionation) at the substrate. The theoretical background for this study, performed by digital simulations using a finite difference method, considers a chemical reaction at the substrate with general stoichiometry. In this case, the fraction of regenerated mediator (ν_S) may differ with respect to a substrate reaction that is the reverse of the tip reaction, resulting in an asymmetric mediator loop. Simulated tip current transients and approach curves at different values of the kinetic rate constant for reactions where $\nu_S < 1$ were used to analyze this new SECM situation. This approach was used to study the catalytic decomposition of hydrogen peroxide ($HO_2^- \rightarrow {}^1/_2O_2 + OH^-$), where $\nu_S = 0.5$, on supported catalysts. A gold−mercury amalgam tip was used to quantitatively reduce dissolved O_2 (mediator) to HO_2^-, which was decomposed back to oxygen at the catalyst substrate. Rate constants for the decomposition reaction on immobilized catalase and Pt particles were measured at different pH values by the correlation of experimental approach curves with the theoretical dependencies.

Introduction

Heterogeneous catalytic reactions at the liquid−solid interface are important in chemistry (e.g., in synthesis and electrode reactions). One important case is the heterogeneous decomposition of hydrogen peroxide into O_2 and OH^- (eq 1) that occurs at a high rate on noble metals such as Pt and its alloys,[1−3] on oxides,[4−7] immobilized complexes[8,9] and enzymes such as catalase.[10−13] There is also interest in H_2O_2 removal from final products and wastes[10−14] and in fundamental studies of the reaction mechanism in electrode reactions, like oxygen electroreduction.[15]

$$2H_2O_2 \rightarrow O_2 + 2H_2O \qquad (1a)$$

or

$$HO_2^- \rightarrow {}^1/_2O_2 + HO^- \text{ (strongly alkaline media)} \qquad (1b)$$

In studying the kinetics of hydrogen peroxide decomposition catalyzed by solids, the catalyst is often dispersed into a solution containing hydrogen peroxide. The concentration of peroxide or the volume of evolved oxygen is monitored with the time over a time frame of hours.[2−14,16] Thus, the heterogeneous rate constant (cm s^{-1}) can be calculated from a pseudo-homogeneous rate constant (s^{-1}) estimated from the dependency of peroxide concentration on time.[17] The method is time-consuming and may require significant amounts of material to reach the desired detection limits. Scanning electrochemical microscopy (SECM) is a good alternative method because of its simple and efficient way of studying many types of surfaces.[18] The usefulness of this technique to the study of electrode reaction kinetics is well-known.[19] Catalyzed heterogeneous processes have been extensively analyzed by SECM, mainly enzyme-assisted reactions[20] and corrosion processes.[21] Chemical reactions catalyzed by metals, such us the reduction of protons by methyl viologen on platinum, have been analyzed by SECM, allowing the direct measurement of the heterogeneous rate constant.[22] Moreover, gas evolution is not necessary, and the quantification is performed through electrochemical signals, significantly more sensitive than the currently used analytical methods.

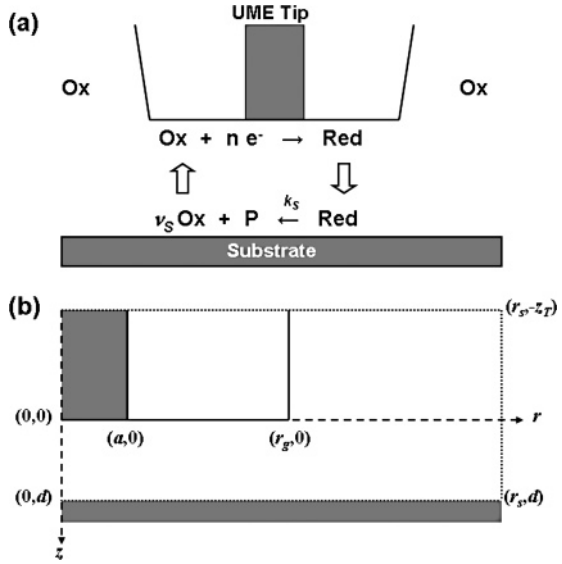

Figure 1. (a) Schematic of the SECM feedback mode operating with a generic asymmetric mediator loop. (b) Cylindrical coordinate system for digital simulations.

The study of catalytic decomposition reactions by SECM is different from earlier studies, and the theoretical formulation for this type of problem has not yet been reported. Figure 1a shows the main difference from the usual system with an electrode reaction at the substrate. In this case, the mediator

10.1021/jp050340c CCC: $30.25
Published on Web 04/12/2005

Ox is electroreduced at the tip under mass-transport control generating Red, which diffuses toward the substrate. The substrate surface catalyzes the decomposition of Red to Ox, which diffuses back to the tip, thus closing the feedback loop. However, because the substrate and tip reactions are different, they may have dissimilar Ox stoichiometric coefficients. As a consequence, the flux of Ox that is regenerated at the substrate will decrease by a factor ν_S with respect to the reverse reaction. Questions that need to be addressed include how the asymmetry in the mediator regeneration affects the transient tip current response and how an approach curve is modified by the value of ν_S. In this paper, we report a theoretical treatment of this system based on a numerical simulation that addresses these issues. Working curves are given to treat experimental results. Finally, to illustrate this approach, we perform an SECM-based kinetic study of hydrogen peroxide decomposition ($\nu_S = 0.5$) in alkaline solution on well-known metal and enzyme immobilized catalysts.

Theory

Consider a typical SECM experiment where the mediator Ox, initially present at a concentration c_{Ox}*, is electroreduced to Red under diffusion control through reaction 2 at the tip. At the substrate, Red undergoes the irreversible first-order chemical reaction 3 catalyzed by the substrate surface that regenerates Ox only partially (depending on the value of ν_S) and other products (P). The rate of this reaction will be a function of the catalytic activity of the substrate material, reflected on the value of the first-order heterogeneous rate constant (k_s in cm s^{-1}).

$$\text{Tip: } \mathrm{Ox} + n\mathrm{e}^- \rightarrow \mathrm{Red} \tag{2}$$

$$\text{Substrate: } \mathrm{Red} \rightarrow \nu_S \mathrm{Ox} + \mathrm{P} \tag{3}$$

The boundary conditions to treat this problem are similar to typical feedback-mode SECM situations with an irreversible reaction at the substrate.[19] They are presented in eqs 4−10 in terms of fluxes of species (J_{Ox}, J_{Red}) for the cylindrical coordinate system defined in Figure 1b. The only difference with previous treatments is the condition at the substrate surface given by eq 9a, which takes into account the effect of a generic stoichiometric coefficient at the substrate reaction.

Initial condition ($t = 0$):

$$0 \le r \le r_s,\ 0 \le z \le d, \text{ and } r_g \le r \le r_s,\ -z_T \le z < 0$$

$$c_{Ox}(r, z) = c_{Ox}^*,\ c_{Red}(r, z) = 0 \tag{4}$$

$t > 0$:

Ultramicroelectode (UME) disk surface: $0 \le r \le a,\ z = 0$

$$c_{Ox}(r, 0) = 0 \tag{5a}$$

$$j_T(r) = nF\, J_{Ox}^{\,z}(r, 0) = -nFD \left.\frac{\partial c_{Ox}(r, z)}{\partial z}\right)_{z=0} \tag{5b}$$

Insulation regions: $a < r \le r_g,\ z = 0$

$$J_{Ox}^{\,z}(r, 0) = J_{Red}^{\,z}(r, 0) = 0 \tag{6a}$$

$$r = r_g,\ -z_T \le z \le 0 \qquad J_{Ox}^{\,r}(r_g, z) = J_{Red}^{\,r}(r_g, z) = 0 \tag{6b}$$

Axis of symmetry: $r = 0,\ 0 \le z \le d$

$$J_{Ox}^{\,r}(0, z) = J_{Red}^{\,r}(0, z) = 0 \tag{7}$$

Space limits: $r_g \le r \le r_s,\ z = -z_T$ and $r = r_s,\ -z_T \le z \le d$

$$c_{Ox}(r, z) = c_{Ox}^*,\ c_{Red}(r, z) = 0 \tag{8}$$

Substrate surface: $0 < r \le r_s,\ z = d$

$$J_{Ox}^{\,z}(r, d) = \nu_s k_s\, c_{Red}(r, d) \tag{9a}$$

$$J_{Red}^{\,z}(r, d) = -k_s\, c_{Red}(r, d) \tag{9b}$$

All other regions:

$$J_{Ox}(r, z) = -D\nabla c_{Ox}(r, z) \tag{10a}$$

$$J_{Red}(r, z) = -D\nabla c_{Red}(r, z) \tag{10b}$$

c_{Ox} and c_{Red} are the concentrations of species Ox and Red, respectively, at the coordinate (r, z), c_{Ox}* is the bulk concentration of Ox, $j_T(r)$ is the tip current density at r, and D is the diffusion coefficient of Ox or Red. The superscript (r or z) on J indicates the direction for the flux. Note that the tip current is defined by eq 11.

$$i_T = 2\pi \int_0^a j_T(r)\, r\, \mathrm{d}r \tag{11}$$

Transient and steady-state approach curves were simulated by a two-dimensional finite difference (FD) method in cylindrical coordinates previously described for another SECM mode.[23] Normalized variables[19] were used in the calculations. The system presented in Figure 1b was mapped into ring-shaped boxes with normalized length and height of 0.02 (no expanding grid was used). Typically, the number of boxes in the r direction that were used in the bulk solution region ($r_g < r < r_s$) was the same as that used beneath the tip surface ($0 < r < r_g$), for example, 250 boxes for an RG = 5, where RG = r_g/a. A total of 500 boxes were used in the z direction in the region $-z_T < z < d$; this number was kept constant regardless of the tip−substrate distance. The normalized time interval ($\tau = tD/a^2$) length was 0.0001. Each calculation started from the initial conditions, and iterations were performed until the normalized tip current ($I = i_T/i_{T,\infty}$, where $i_{T,\infty} = 4nFDac_{Ox}$*) changed less than 10^{-6}/step. This situation was considered to be the steady-state condition, and that value of I was recorded as a function of the normalized tip−substrate distance ($L = d/a$). To perform the simulation at a new distance (to make complete approach curves), the tip−substrate distance was decreased by removing a full row of boxes from the center of the tip−substrate gap. The steady-state concentration values in each remaining box, that were calculated at the previous distance, were used as initial conditions. That procedure speeded up the attainment of the new steady-state situation. All the data presented in this work are tabulated as Supporting Information.

Experimental Details

Chemicals and Materials. A gold wire of 25-μm diameter was obtained from Goodfellow (Devon, PA). Bovine liver catalase (EC 1.11.1.6) powder from Sigma-Aldrich (Saint-Louis, MO) was used without further purification. Triethyloxonium tetrafluoroborate (TOTFB), 1,4-diaminobutane (DAB), dichloromethane, and methanol from Sigma-Aldrich were used as received. Glutaraldehyde was obtained in nitrogen-filled ampules of 8% (v/v) aqueous solutions at electron microscopy grade from Polysciences, Inc. (Warrington, PA). The nylon samples used

(Durethan A30) were 1-cm-diameter, 3-mm-thick disks (Bayer Corp., Pittsburgh, PA). Prior to each sample preparation, the shaped disks were cleaned by ultrasonication in methanol for 30 min followed by 30 min ultrasonication in water. 3-Mercaptopropyltrimethoxysilane (MPTS) was from Sigma-Aldrich (Saint-Louis, MO). Sodium borohydride ($NaBH_4$) and hexachloroplatinic acid (H_2PtCl_6) were used as received from Alfa Aesar (Ward Hill, MA). All glassware was cleaned in 70/30 HNO_3/H_2SO_4 before use. Milli-Q purity water was used.

SECM Probes. Gold−mercury amalgam 25-μm-diameter UME disks were used as SECM tips. They were prepared following the procedure described by Mandler et al.[22] A 25-μm-diameter gold disk tip is prepared by heat-sealing a gold wire into a borosilicate glass capillary following the standard procedure previously described.[18] The tip is then polished and sharpened. Then, mercury is electrodeposited on the Au disk from a 0.1 M $HgNO_3$ (Alfa Aesar) solution at −0.2 V vs Hg/Hg_2SO_4 for 3 min. This procedure generates an Hg hemisphere deposited on the Au disk. A rough and soft Au−Hg amalgam is spontaneously formed onto the electrode in less than 5 min. To make a smooth disk of this material, the tip is softly polished over a polishing cloth containing a diluted dispersion of alumina 0.05 μm in water, rinsed thoroughly with water, and cleaned by ultrasonication for 30 s.

SECM Substrates. *Catalase Immobilized on Nylon.* A modified Morris O-alkylation[24] can be used to immobilize the protein on the nylon surface through external free amine groups. However, because of the high number of accessible free lysine residues on the catalase, the protein will not adopt a preferred orientation once on the surface. First, the nylon surface was activated by immersion in 0.1 M TOTFB in dichloromethane for 6 min. This step also removed any aged layer on top of the nylon disks. After rinsing with methanol, the disks were immersed in a 1 M DAB solution in 0.1 M carbonate buffer (pH = 9.8) and left at room temperature for 20 h in a calcium chloride desiccator. After thorough rinsing in the same carbonate buffer, the samples were immersed in 4% (v/v) glutaraldehyde in 20 mM phosphate buffer (pH = 8.1) for 3 h. Another rinsing step in the same phosphate buffer preceded the enzyme coupling. A drop of a 6 mg/mL (96 μM) catalase solution in 0.1 M carbonate buffer (pH = 9.8) was deposited on the treated nylon disk surfaces for 30 min at room temperature. The catalase solution was finally diluted to 2 mg/mL with buffer and left for 20 additional immersion hours at room temperature in a calcium chloride desiccator. Finally, the disks were rinsed with and stored in 0.1 mM carbonate buffer (pH = 9.8) for not more than 3 h.

Platinum Particles Immobilized on Glass. Platinum nanoparticles were synthesized and immobilized on 1-mm-thick plain glass microscope slides (Fisher Scientific, Pittsburgh, PA) via silanization with a thiol-terminated molecule. A 10 mM $NaBH_4$ solution was added dropwise to a 2.6 mM H_2PtCl_6 solution under stirring, reducing the Pt salt to nanometer-sized Pt particles in suspension.[25] $NaBH_4$ was added until the solution showed a persistent yellow-gray color. Completion of this process was checked by UV−vis spectroscopy. The glass supports were prepared as follows: New glass microscope slides were cleaned in a 30/70 H_2O_2/H_2SO_4 solution heated to 80 °C for 20 min, rinsed with water, and dried at 100 °C. They were then immersed in a 1% (v/v) MPTS solution in methanol for 20 h at room temperature in a calcium chloride desiccator. After intense rinsing with methanol, they were placed in the fresh platinum colloidal suspension for 3 h at room temperature. Finally, they were rinsed with water and used immediately.

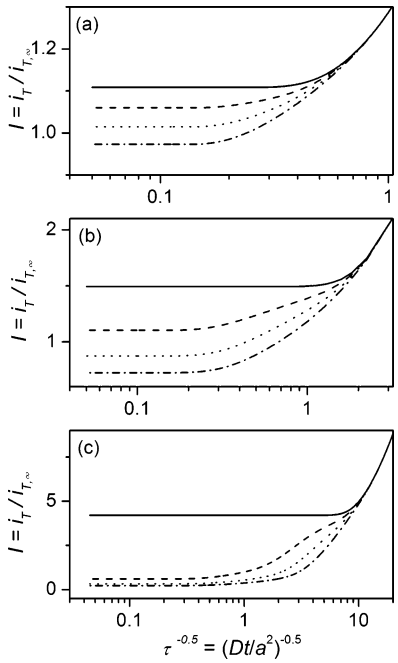

Figure 2. Normalized tip current transients calculated from FD simulations at L = 3.0 (a), 1.0 (b), and 0.2 (c) (top to bottom) for ν_S = 1 (solid lines), 0.75 (dashed), 0.5 (dotted), 0.25 (dash−dotted).

Measurements. The electrochemical studies were performed in 0.2 M phosphate solutions of different pH values in the range $6 \leq pH \leq 12$ at room temperature with a three-electrode cell, using an Au−Hg tip as the SECM probe, a Pt wire as the counter electrode, and Hg/Hg_2SO_4 as the reference electrode (Radiometer Analytical, France). The substrate was tightened at the bottom of the Teflon cell via an FETFE O-ring. SECM measurements were carried out using a CHI 900 microscope (CH Instruments, Austin, TX). Examination of Pt-immobilized glass surfaces was performed by atomic force microscopy (AFM) in the tapping mode with a Veeco Dimension 3100 microscope and a Nanoscope IV controller (Veeco Instruments, Inc., Santa Barbara, CA) in air at room temperature. Standard commercial silicon-etched probes (Nanosensors Point Probe Plus NCH, Switzerland) with a nominal spring constant of 21−78 N m^{-1} were used. They typically had a resonant frequency of around 265 kHz with a quality factor of about 450. To obtain a pure attractive regime and reduce the effect of the damping of the oscillation near the surface, a frequency smaller than the resonant frequency for which the phase delay was equal to $-\pi/4$ was used, and the free oscillation amplitude for that frequency was adjusted to values typically slightly smaller than 10 nm until the phase signal was characteristic of an intermittent contact situation in a purely attractive field.[26] This also allowed the exclusion of initial tip pollution before imaging the surface.

Results and Discussion

Simulations. Transients of the tip current for a diffusion-controlled ($k_S \rightarrow \infty$) first-order reaction at the substrate are plotted in Figure 2 for different tip−substrate distances and different stoichiometric coefficients. These simulations were performed for a tip with RG = 5, and the tip current values were normalized taking into account the effect of RG on the value of $i_{T,\infty}$.[27] It is clear that the tip current reaches a steady-state value in all cases, and the time to reach this steady state depends on the L and ν_S values. The smaller the ν_S value, the more time is necessary for the tip current to reach the steady-state value. For example, at a distance L = 1, it takes a

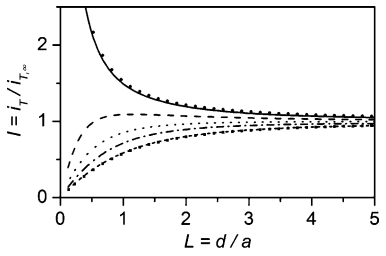

Figure 3. Steady-state SECM approach curves calculated from FD simulations for the substrate reaction operating under diffusion control ($\kappa \rightarrow \infty$) at different values of ν_S: (top to bottom) 1.0 (solid line), 0.75 (dashed), 0.5 (dotted), 0.25 (dash−dotted), 0.0 (short-dashed). Theoretical diffusion-controlled positive (●) and negative (■) feedback approach curves given earlier for $\nu_S = 1.0$[27] are included as reference curves. Tip RG = 5.

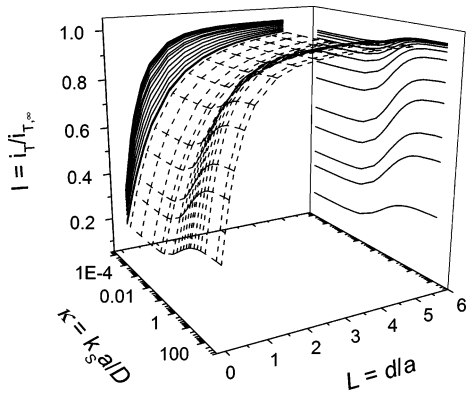

Figure 4. Steady-state normalized dependence of the tip current (I) on the substrate heterogeneous rate constant (κ) and tip−substrate distance (L). I vs L projections (approach curves) correspond (from bottom to top) to $\kappa = 100$, 50, 10, 5, 3, 1.8, 1, 0.75, 0.5, 0.3, 0.18, 0.1, 0.05, 0.01, 10^{-3}, 10^{-4}, and 10^{-5}. I vs κ projections correspond (from top to bottom) to $L = 5$, 4.52, 4, 3.52, 3, 2.52, 2, 1.52, 1, 0.76, 0.52, 0.4, and 0.2.

normalized time $\tau = 3$ (typically ~30 ms for a 1-μm-diameter UME) to reach steady state when $\nu_S = 1$, but it takes $\tau = 40$ (~400 ms for a 1-μm UME) when $\nu_S = 0.5$. Thus, experimental approach curves must be measured at smaller approach rates than usually used to ensure steady-state conditions at each point. An important approximation in these calculations is the assumption of similar diffusion coefficients for Ox and Red, whereas in real situations, they may differ significantly, which would affect the quantitative interpretation of results to some extent.[28]

Simulated steady-state approach curves for reactions operating under total diffusion control ($k_S \rightarrow \infty$), for different values of ν_S, are shown in Figure 3. The curve calculated for $\nu_S = 1$ agrees with those previously reported for total positive feedback (RG = 5) for an electrode reaction at the substrate (●),[27] and the curve for $\nu_S = 0$ is similar to that corresponding to an insulating surface (■).[27] For intermediate values of ν_S, the feedback due to regeneration of the tip reactant decreases dramatically when ν_S decreases from 1 to 0.5, and below $\nu_S = 0.5$, the sensitivity of the approach curves to ν_S is poor. The situation for $\nu_S = 0.5$, relevant to the analysis of the hydrogen peroxide decomposition and typical of many disproportionation reactions, was analyzed in detail. Figure 4 shows the simulated dependence $I = I(L, \kappa)$ for $\nu_S = 0.5$, where κ is the normalized rate constant ($\kappa = k_S a/D$) of the reaction at the substrate. The I versus κ projections indicate that I is insensitive to the κ value when $\kappa \geq 10$ and $\kappa \leq 10^{-3}$. This is also observed in the I versus L projections (approach curves), where all the curves for $\kappa \geq 1$ correspond to total positive feedback for that value of ν_S, while for $\kappa < 10^{-3}$, the approach curves correspond to an insulating surface. For the range $10 > \kappa > 10^{-3}$, the $I-\kappa$ slope is significant, and thus, the approach curves are very sensitive to the κ value. Thus, in this domain of reaction rates, the rate constant can be determined by fitting the experimental approach curves.

For processing experimental results, analytical equations are more useful and easier to use than working curves. For this reason, the simulated dependencies $I = I(L, \kappa)$ shown in Figure 4 were fit to the empirical eq 12, which reproduces the simulated data (see Supporting Information) with an error of less than 0.5%. Although this equation does not have a physical meaning, it is very useful in treating experimental approach curves (I vs L), since κ is then the only adjustable parameter.

$$I = \frac{A_1 - A_2}{1 + \left(\frac{\kappa}{A_3}\right)^{A_4}} + A_2 \tag{12}$$

$$A_1 = -0.00245 + 0.907\left[1 - \exp\left(-\frac{L}{0.99}\right)\right] + 3.328 \times 10^7\left[1 - \exp\left(-\frac{L}{3.637 \times 10^9}\right)\right] \tag{13}$$

$$A_2 = -0.0028 + 0.972\left[1 - \exp\left(-\frac{L}{0.487}\right)\right] + 0.0447\left[1 - \exp\left(-\frac{L}{5.05}\right)\right] \tag{14}$$

$$A_3 = \frac{0.261}{\left(\frac{0.214}{L} + 1\right)} + 0.222 \exp\left[-\frac{(L + 0.034)}{1.195}\right]\left\{1 - \exp\left[-\frac{(L + 0.034)}{0.236}\right]\right\}^{3.48} \tag{15}$$

$$A_4 = 0.7826 + 0.22\left[1 - \exp\left(-\frac{L}{1.384}\right)\right] \tag{16}$$

Study of Hydrogen Peroxide Decomposition. The decomposition (disproportionation) of hydrogen peroxide (eq 1) catalyzed by solid surfaces is a case where $\nu_S = 0.5$. It can be studied by this SECM approach by electrogenerating H_2O_2 or HO_2^- from dissolved O_2 at a tip where the 2e reduction takes place and monitoring the feedback of O_2 from the substrate, according to the scheme in Figure 5a.

Tip Preparation and Characterization., Mercury is a good electrode material to carry out exclusively the two-electron (2e) reduction of O_2 to HO_2^- under diffusion control at the tip, because it produces two very well separated current plateaus for two-electron (2e) and four-electron (4e) reductions of O_2.[29] While hemispheric Hg tips have been used as SECM probes,[29,30] their application in this study is not convenient, because the feedback sensitivity would be significantly lower than with a disk.[31] Moreover, the theoretical background in the previous section was developed for a disk electrode. While solid electrode tips such as gold and carbon can be efficient generators of HO_2^- from O_2,[32,33] at low pH (<8), the 4e pathway becomes significant before the 2e pathway reaches the limiting current. A solid material that possesses the electrochemical properties of mercury is the amalgam Au−Hg, which has already been used as an SECM disk probe.[22] As described in the Experimental Details section, its preparation by electrodeposition of Hg on an Au tip is straightforward. Cyclic voltammograms with an

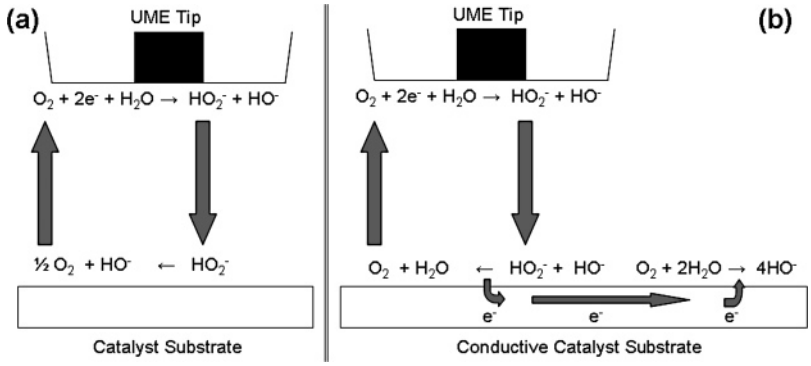

Figure 5. (a) Schematic of the tip−substrate O_2/HO_2^- feedback process to study the hydrogen peroxide decomposition reaction by SECM. (b) Schematic of the effect of the lateral reaction involving electron transfer (O_2 electroreduction) on the tip−substrate O_2/HO_2^- feedback process.

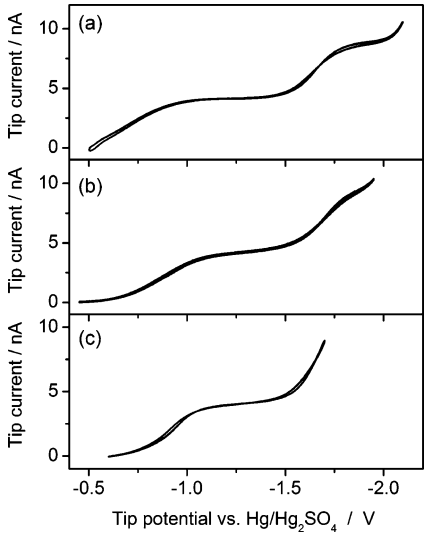

Figure 6. Cyclic voltammogram of a Au−Hg amalgam tip (25-μm diameter) in air-saturated 0.2 M phosphate solution at pH = 12.0 (a), 7.1 (b), and 5.0 (c). Scan rate: 0.1 V s^{-1}.

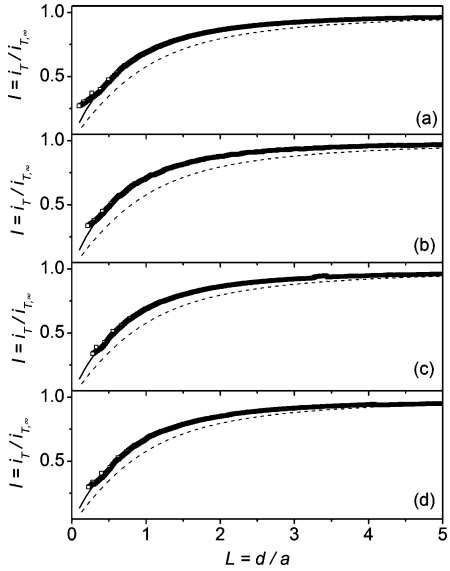

Figure 7. Experimental approach curves (□) measured on immobilized catalase−nylon substrate using the O_2/H_2O_2 mediator feedback to an Au−Hg amalgam tip (25-μm diameter, RG ≅ 5) in air-saturated 0.2 M phosphate solutions of pH = 5.5 (a), 7.1 (b), 9.1 (c), and 10.3 (d). Scan rate: 1 μm s^{-1}. Solid lines are the theoretical I vs L dependencies generated from eq 12 using the κ values resulting from the best correlations with the experimental results for κ = 0.1521 (a), 0.2555 (b), 0.1667 (c), and 0.1218 (d). The theoretical negative feedback approach curve for a tip with RG = 5 (dashed line)[27] is included as a reference.

Au−Hg tip in air-saturated 0.2 M phosphate solutions at different pH values (12, 7.1, and 5) are shown in Figure 6. In alkaline solution, one can clearly identify two waves with half-wave potentials of −0.9 V and −1.7 V for the overall 2e and 4e reduction of O_2, respectively, before hydrogen evolution occurs. As the solution pH decreases, the hydrogen evolution reaction overlaps the 4e O_2 reduction, but the 2e process is still well-defined. At the anodic limit of ∼−0.5 V, mercury oxidizes to HgO in alkaline solutions. These voltammograms indicate that the 2e reduction of oxygen is diffusion-controlled at a 25-μm diameter Hg−Au disk tip at −1.25 V versus Hg/Hg_2SO_4 with a limiting current $i_{T,\infty} = 4.0 \pm 0.1$ nA. This value agrees with the UME current of 3.95 nA that is calculated from the equation for the UME disk limiting current ($i_{T,\infty} = 4nFDac$),[34] assuming an oxygen diffusion coefficient $D = 1.5 \times 10^{-5}$ cm^2/s and a solubility c = 0.27 mM at 0.21 atm in phosphate solutions.[35]

Hydrogen Peroxide Decomposition on Immobilized Catalase. Bovine liver catalase specifically catalyzes the conversion of hydrogen peroxide to oxygen and water. It is a homotetrameric hemoprotein[36] of a subunit (molecular weight = 60 000−65 000) with 27 lysine residues. A large portion (21) of them are located on the external protein surface and are therefore accessible for surface chemistry.[37] This enzyme, immobilized on different surfaces such as polymer and oxide pellets, is used for the elimination of hydrogen peroxide from industrial fluids such as textile effluents and food products.[10−14] Thus, the described SECM approach was applied as a demonstration to study this type of material. Some approach curves obtained on nylon-immobilized catalase in 0.2 M phosphate solutions at different pH values using a 25-μm Au−Hg tip with RG ≅ 5 are presented in Figure 7 (symbols). These curves were measured at a scan rate of 1 μm s^{-1}, which is sufficiently slow to ensure that steady-state conditions are reached for each point. At each pH value, the approach curves were measured on 3 different spots on the substrate surface separated by ∼400 μm. Then, the cell was thoroughly rinsed with the new solution and refilled. After 10 min, a new set of 3 approach curves was taken. The correlations of these approach curves using eq 12 (solid lines) are shown in Figure 7 on top of the respective experimental points. Even when O_2 feedback is small, the approach curves clearly differ from the curve obtained on an inert surface, and it is possible to extract precise values of the rate constant. To perform the fitting, experimental $i_{T,\infty}$ and offset distance values must be estimated first.[18] This is performed by overlapping the approach curve over a family of simulated curves, manually adjusting these two parameters in a narrow, physically meaningful range. Once these two parameters are established, the value of κ is calculated by nonlinear correlation of the experimental curve with eq 12.

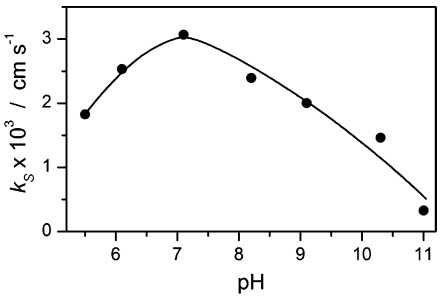

Figure 8. Dependence of the hydrogen peroxide decomposition heterogeneous rate constant (k_S) on the pH, measured by SECM on immobilized catalase−nylon substrate in air-saturated 0.2 M phosphate solutions.

Figure 8 shows the dependence of the rate constant (cm s^{-1}) determined on immobilized catalase on the pH. Each point is the mean value of 3 measurements. To convert the dimensionless rate constant (κ) measured from the approach curves into the k_S value, values of $D = 1.5 \times 10^{-5}$ cm^2 s^{-1} [35] and $a = 12.5 \times 10^{-4}$ cm were used. The highest activity is observed at around pH = 7, in agreement with results obtained on catalase immobilized on alumina pellets and chitosan beads.[10−13] The catalyst became deactivated after testing at pH > 12, probably because the amide bonds to the nylon surface were irreversibly hydrolyzed at that pH value. A comparison of the values obtained in this work with the results reported for immobilized catalase[11] is not directly possible because of the lack of information to convert the reported apparent pseudo-homogeneous rate constants (k', in s^{-1}) into k_S. If nylon-immobilized catalase (10-μm-radius pellets, specific area = 2.6 cm^2 mg^{-1}) operates in a discontinuous reactor similar to that used by Tarhan et al. (60 mg in 20 mL of solution),[11] it would have a pseudo-homogeneous rate constant $k' = 2.3 \times 10^{-2}$ s^{-1} at pH = 7 derived from the value of k_S measured by our technique. This value agrees very well with those reported for immobilized catalase on other materials such as alumina ($k' = 1.6 \times 10^{-2}$ s^{-1}) and polymer pellets ($k' = 7.8 \times 10^{-3}$ s^{-1}).[11] On the other hand, the calculated k_S values, between 1×10^{-3} and 3×10^{-3} cm s^{-1}, are similar to those found on other immobilized enzymes for other reactions, such as glucose oxidase for the oxidation of glucose.[38]

Hydrogen Peroxide Decomposition on Immobilized Pt Nanoparticles. Pt is a very efficient material for decomposing hydrogen peroxide, and studies of its activity (mechanism, pH dependency, effects of alloying) have been reported since the middle of the past century.[1] In this work, Pt nanoparticles were immobilized on silanized glass surfaces from dilute colloid solutions prepared by reduction of H_2PtCl_6 with $NaBH_4$. UV−vis spectroscopy was used to check for the completion of platinum reduction. $PtCl_6^{2-}$ shows a strong absorption peak at 260 nm, which disappears once the reduction with an excess of $NaBH_4$ is complete.[39] A remaining broad absorption signal was observed after completion of the reaction, characteristic of light scattering by colloidal solutions.[40] The conductivity of this surface was analyzed by performing SECM approach curves using the oxidation of ferrocene methanol. On conductive surfaces, the reduction of tip-generated ferrocenium is driven at the substrate at open circuit potential because of a lateral electron transfer process.[41] Thus, a positive approach curve is expected on a conductive surface. However, pure negative feedback was observed in the approach curves obtained on the Pt-immobilized samples under such conditions, which reveals a surface with essentially no contact between the small conductive particles. AFM scans of the immobilized material (Figure 9) show a surface roughened by particle immobilization. The particles have an average apparent lateral diameter of 40−50 nm. However, lateral sizes can generally not be trusted in AFM experiments because of tip convolution. The apparent height of the particles is about 4−5 nm, but this value is uncertain, because the height reference (glass surface) is not clear in the scan because of limitations from the tip size. We therefore estimate an average particle slightly larger than 5 nm. The AFM scan also shows several types of aggregates made of 2−5 particles on the surface. Aggregation is caused by the absence of capping agent during the synthesis step. Nevertheless, the platinum particles covering the glass surface are clearly not totally interconnected. For instance, in the surface cross-section in Figure 9, the central 200-nm wide structure delimitated by the black symbols is separated from the neighboring aggregates by 15-nm-wide gaps. Several wider gaps also appear in the probed area. Therefore, the surface is essentially insulating over the micrometer range, explaining the SECM results previously described.

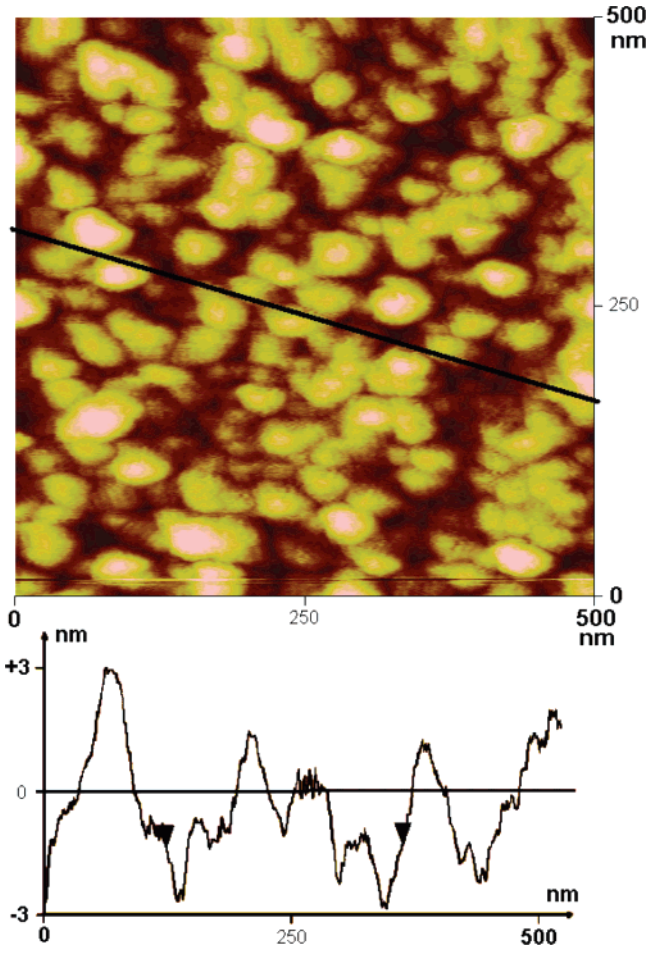

Figure 9. Top image: Tapping mode AFM image of Pt nanoparticles chemically immobilized on glass. The image is flattened to the second order to remove tilt and scan curvature artifacts. Height scale: 0−6 nm. Bottom graph: Cross-section along the black line in the AFM image.

The activity of these surfaces for hydrogen peroxide decomposition at different pH values was examined by the described SECM approach. The approach curves measured on these surfaces at different pH values showed significant activity for this reaction, as shown in Figure 10 (symbols). They were correlated with eq 12 (solid lines), following the same procedure described for immobilized catalase to calculate the heterogeneous rate constants. The activity of immobilized Pt particles

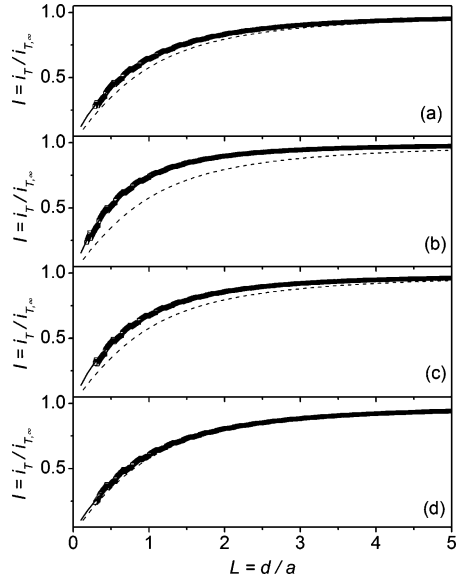

Figure 10. Experimental approach curves (□) measured on immobilized Pt nanoparticles glass using the O_2/HO_2^- mediator feedback to an Au−Hg amalgam tip (25-μm diameter, RG ≅ 5) in air-saturated 0.2 M phosphate solutions of pH = 12.8 (a), 11.9 (b), 11.3 (c), and 9.56 (d). Scan rate: 1 μm s^{-1}. Solid lines are the theoretical I vs L dependencies generated from eq 12 using the κ values resulting from the best correlations with the experimental results for $\kappa = 0.0706$ (a), 0.4181 (b), 0.1472 (c), and 0.0165 (d). The theoretical negative feedback approach curve for a tip with RG = 5 (dashed line)[27] is included as a reference.

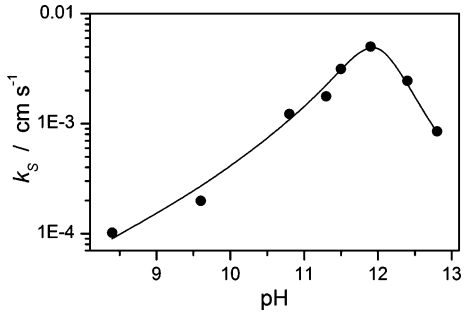

Figure 11. Dependence of the hydrogen peroxide decomposition heterogeneous rate constant (k_S) on the pH, measured by SECM on chemically immobilized Pt particles (5−10-nm diameter) over glass, in air-saturated 0.2 M phosphate solutions.

shows a maximum at pH ≅ 12 ($k_S = 5 \times 10^{-3}$ cm s^{-1}), as shown in Figure 11, similar to other noble metals.[2] The value of k_S at nearly neutral pH is 10^{-4} cm s^{-1}, close to $\sim 1.6 \times 10^{-4}$ cm s^{-1} determined on Pt black.[2]

The Problem of Lateral Electron Transfer on Conductive Surfaces. There is a limitation when this SECM approach is applied to study hydrogen peroxide decomposition on conductive surfaces that are active for oxygen electroreduction, for example, a Pt sheet. The open circuit potential of Pt and other electrode surfaces such as Au and carbon in air-saturated phosphate solution is a mixed potential at about −0.5 V versus Hg/Hg_2SO_4 (depending on the material and the solution pH). This potential is governed by the interaction between dissolved oxygen and the electrode surface.[15] When a small fraction of the electrode area (underneath the tip) is exposed to hydrogen peroxide, a corrosion process occurs which is schematically presented in Figure 5b. Hydrogen peroxide is electrooxidized to oxygen at this electrode potential, while dissolved oxygen is electroreduced to water on the rest of the electrode surface. The corrosion current of this process is so small that large-area

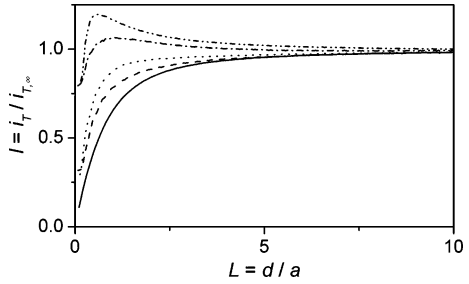

Figure 12. Experimental approach curves obtained on smooth Pt disks with different radii (a_S) at open circuit potential, using the O_2/HO_2^- mediator feedback to an Au−Hg amalgam tip (25-μm diameter, RG ≅ 5) in air-saturated 0.2 M phosphate solutions of pH = 12.0. a_S = 12.5 μm (dashed), 25 μm (dotted), 62.5 μm (dash−dotted), 0.5 mm (dash−dot−dotted). Scan rate: 1 μm s^{-1}. Solid line: negative feedback approach curve.

electrodes are able to sustain the process even when they are poor catalysts for oxygen electroreduction. Thus, the feedback of oxygen observed at the tip is, in fact, generated in the electrooxidation of hydrogen peroxide at that potential, which is a process with $\nu_S = 1$. Thus, the approach curves measured on large conductive electrodes, for example, those shown in Figure 12 for a substrate with radius $a_s = 0.5$ mm, do not represent the decomposition reaction but rather the electrooxidation reaction. However, as the electrode area becomes smaller and comparable to the tip-affected area, this process is less significant, as shown in Figure 12, and is negligible, as expected when the substrate is about the size of the tip.[19] For this last condition, however, a new theoretical treatment considering the effect of substrate size would be necessary to correlate the experimental approach curves for hydrogen peroxide decomposition measured on small substrates ($a_s \cong a$). If the catalyst is deposited on an insulator surface (e.g., glass or nylon) as described here, the problem of substrate size does not arise.

Conclusion

We have demonstrated the use of SECM operating with an asymmetric feedback loop to study heterogeneous chemical reactions in liquid solutions. Results from digital simulations verified that even when there is an asymmetry between the reactions at the tip (electrode reaction) and at the substrate (chemical reaction) a steady-state feedback process is reached. The feedback-affected tip current is strongly dependent on the stoichiometry of the substrate reaction relative to the tip reaction. The dependence of steady-state tip current versus tip−substrate distance can be used to determine the rate constant of the chemical reaction, similarly to the classical procedure for SECM kinetic studies of electron transfer processes. The use of this approach was demonstrated in the study of hydrogen peroxide decomposition on different types of well-known catalysts including enzymatic and metallic materials. Catalase-modified nylon surfaces show significant activity ($k_S \cong (1-3) \times 10^{-3}$ cm s^{-1}) in the pH range 5 < pH < 10, well covered by the detection limits of this technique, with a maximum at pH = 7.05. Pt particles (5−10 nm average diameter) immobilized on silanized glass present optimum activity for this reaction at pH = 11.9 with an apparent rate constant ($k_S \cong 5 \times 10^{-3}$ cm s^{-1}). This material retains its good activity in the pH range 10 < pH < 13. Conductive surfaces can be studied by this technique only if the size of the analyzed substrate is decreased to the dimensions of the tip probe. Otherwise, the electrooxidation of hydrogen peroxide driven at the substrate open circuit potential would interfere with the measurements.

Acknowledgment. This work has been supported by grants from the National Science Foundation (CHE 0109587) and SPRING. Durethan A-30 samples were a kind gift from Dr. George Kriek at the Bayer Corporation. C.H. acknowledges a grant from the French Ministry of Research and the Centre National de la Recherche Scientifique. J.L.F. thanks the Fundación Antorchas (Argentina) for a postdoctoral fellowship.

Supporting Information Available: Simulation results of normalized tip current at different normalized tip−substrate distances and heterogeneous rate constants obtained for a tip with RG = 5. This material is available free of charge via the Internet at http://pubs.acs.org.

References and Notes

(1) Zubovich, I. A. *Zh. Fiz. Khim.* **1955**, *29*, 917.
(2) McKee, D. W. *J. Catal.* **1969**, *14*, 355.
(3) Pirault-Roy, L.; Kappenstein, C.; Guerin, M.; Eloirdi, R.; Pillet, N. *J. Propul. Power* **2003**, *18*, 1235.
(4) Ariafard, A.; Aghabozorg, H. R.; Salehirad, F. *Catal. Commun.* **2003**, *4*, 561.
(5) Falcón, H.; Carbonio, R. E.; Fierro, J. L. G. *J. Catal.* **2001**, *203*, 264.
(6) Lysova, A. A.; Kuz′min, A. O.; Parmon, V. N. *Kinet. Catal.* **2003**, *44*, 86.
(7) Vago, E. R.; Calvo, E. J. *J. Electroanal. Chem.* **1995**, *388*, 161.
(8) Labadi, I.; Szilagyi, I.; Jakab, N. I.; Hernadi, K.; Palinko, I. *Mater. Sci.* (*Poland*) **2003**, *21*, 235.
(9) Tarasevich, M. R.; Zakharkin, G. I. *React. Kinet. Catal. Lett.* **1977**, *6*, 77.
(10) Çetinus, S. A.; Öztop, H. N. *Enzyme Microb. Technol.* **2003**, *32*, 889.
(11) Tarhan, L. *Appl. Biochem. Biotechnol.* **1991**, *31*, 109. (b) Tarhan, L.; Uslan, H. *Process Biochem.* **1990**, 14.
(12) Costa, S. A.; Tzanov, T.; Para, A.; Gudelj, M.; Gübitz, G. M.; Cavaca-Paulo, A. *Enzyme Microb. Technol.* **2001**, *28*, 815.
(13) Costa, S. A.; Tzanov, T.; Carneiro, F.; Gübitz, G. M.; Cavaca-Paulo, A. *Biotechnol. Lett.* **2002**, *24*, 173.
(14) Akertek, E.; Tarhan, L. *Appl. Biochem. Biotechnol.* **1995**, *50*, 291.
(15) Adzic, R. In *Electrocatalysis*; Lipkowski, J., Ross, P. N., Eds.; Wiley-VCH: New York, 1998; Chapter 5, p 197.
(16) Mueller, S.; Rieder, H.-D.; Stremmel, W. *Anal. Biochem.* **1997**, *245*, 55.
(17) Vetter, T. A.; Philip Colombo, D., Jr. *J. Chem. Educ.* **2003**, *80*, 788.
(18) *Scanning Electrochemical Microscopy*; Bard, A. J., Mirkin, M. V., Eds.; Marcel Dekker: New York, 2001.
(19) Bard, A. J.; Mirkin, M. V.; Unwin, P. R.; Wipf, D. O. *J. Phys. Chem.* **1992**, *96*, 6, 1861.
(20) Wittstock, G. *Fresenius' J. Anal. Chem.* **2001**, *370*, 303.
(21) Serebrennikova, I.; Lee, S.; White, H. S. *Faraday Discuss.* **2002**, *121*, 199.
(22) Selzer, Y.; Turyan, I.; Mandler, D. *J. Phys. Chem. B* **1999**, *103*, 1509.
(23) Fernández, J. L.; Bard, A. J. *Anal. Chem.* **2004**, *76*, 2281.
(24) Thompson, R. O.; Mandoke, C. S.; Womack, J. P. *Anal. Lett.* **1985**, *18*, 93.
(25) Sarathy, K. V.; Raina, G.; Yadav, R. T.; Kulkarni, G. U.; Rao, C. N. R. *J. Phys. Chem. B* **1997**, *101*, 9876.
(26) Nony, L.; Boisgard, R.; Aimé, J.-P. *J. Chem. Phys.* **1999**, *111*, 1615.
(27) Amphlett, J. L.; Denuault, G. *J. Phys. Chem. B* **1998**, *102*, 9946.
(28) Martin, R. D.; Unwin, P. R. *Anal. Chem.* **1998**, *70*, 276.
(29) Ciani, I.; Burt, D. P.; Daniele, S.; Unwin, P. R. *J. Phys. Chem. B* **2004**, *108*, 3801.
(30) Mauzeroll, J.; Hueske, E. A.; Bard, A. J. *Anal. Chem.* **2003**, *75*, 3880.
(31) Selzer, Y.; Mandler, D. *Anal. Chem.* **2000**, *72*, 2383.
(32) Damjanovic, A.; Genshaw, M. A.; Bockris, J. O. *J. Electroanal. Chem.* **1967**, *15*, 173.
(33) Taylor, R. J.; Humffray, A. A. *J. Electroanal. Chem.* **1975**, *64*, 85.
(34) Wightman, R. M.; Wipf, D. O. In *Electroanalytical Chemistry*; Bard, A. J., Ed.; Marcel Dekker: New York, 1989; Vol. 15, pp 267−353.
(35) Lawson, D. R.; Whiteley, L. D.; Martin, C. R.; Szentirmay, M. N.; Song, J. I. *J. Electrochem. Soc.* **1988**, *135*, 2247.
(36) McPherson, A.; Rich, A. *Arch. Biochem. Biophys.* **1973**, *157*, 23.
(37) Ko, T. P.; Jay, D.; Malkin, A.; McPherson, A. *Acta Crystallogr., Sect. D* **1999**, *55*, 1383. Protein data bank 4BLC.
(38) Pierce, D. T.; Unwin, P. R.; Bard, A. J. *Anal. Chem.* **1992**, *64*, 1795.
(39) Liu, Z.; Ling, X. Y.; Lee, J. Y.; Su, X.; Gan, L. M. *J. Mater. Chem.* **2003**, *13*, 3049.
(40) Furlong, D. N.; Launikonis, A.; Sasse, W. H. F. *J. Chem. Soc., Faraday Trans. 1* **1984**, *80*, 571.
(41) Macpherson, J. V.; Slevin, C. J.; Unwin, P. R. *J. Chem. Soc., Faraday Trans.* **1996**, *92*, 3799.